Climate and Variability in the First Quasi-equilibrium Tropical Circulation Model

Ning Zeng

J. David Neelin

Department of Atmospheric Sciences and
Institute of Geophysics and Planetary Physics
University of California, Los Angeles

Chia Chou

Johnny Wei-Bing Lin

and Hui Su

Department of Atmospheric Sciences
University of California, Los Angeles

April 21, 1999

Abstract

We review the development of a new type of model for simulation and theory of the tropical atmospheric component of climate variations. These models are referred to as "quasi-equilibrium tropical circulation models", or QTCMs, because they make use of approximations associated with quasi-equilibrium (QE) convective parameterizations originally proposed by Arakawa and Schubert. The formulation uses a Galerkin framework in the vertical, but with basis functions tailored to quasi-equilibrium deep convective physics via analytical solutions. The first of these (QTCM1) retains a single vertical structure of temperature and humidity. For a balanced treatment of dynamics and sub-grid scale physics, a physics parameterization package of intermediate complexity is developed. This includes a linearized longwave radiation scheme, a simple cloud prediction method, simple shortwave radiation schemes, and an intermediate land-surface model.

The QTCM1 climatology has a reasonable spatial pattern and seasonal evolution of the tropical convergence zones, including over land regions. The outgoing longwave radiation and net surface heat flux are simulated satisfactorily. The intraseasonal oscillation is largely excited by midlatitude disturbances and is influenced by the evaporation-wind feedback mechanism. The Asian monsoon is slightly weak but depicts the northward progression of the monsoon onset, and a monsoon wind shear index exhibits interannual variability associated with observed SST. The extent and position of the main El Niño/Southern Oscillation rainfall anomalies are simulated, as well as a number of the observed tropical and subtropical teleconnections. The seasonal cycle and interannual variability of the Amazon water budget illustrate reasonable simulation of the hydrologic cycle. While the results are imperfect with respect to observations, many aspects are comparable to GCMs of the previous generation. Considering the complexity of these simulated phenomena, the model is computationally light and easy to diagnose. Sensitivity experiments show that the convective time scale that controls departures from QE has little impact on the climatology, although it can influence fast waves. The model helps to demonstrate the usefulness

of QE thinking not only as a powerful concept, but also as a basis for quantitative simulation of tropical climate and variability.

1. Introduction

Quasi-equilibrium (QE) convective closures for the relation between moist convection and large-scale dynamics originally proposed by Arakawa and Schubert (1974) assert that convective ensembles at scales smaller than the Reynolds average (sub-Reynolds scales) act to remove convective instability within the vertical column (conditional instability of the first kind). The convective motions thus tend to establish a statistical equilibrium between the variables that affect parcel buoyancy, i.e., the large scale temperature and moisture, when an ensemble average is taken over a convective region (Arakawa 1993; Emanuel et al. 1994).

A new class of model for the tropical circulation is proposed (Neelin and Zeng 1998, NZ hereafter; Zeng et al. 1998, ZNC hereafter) that directly exploits constraints placed on the flow by deep convection, as represented by quasi-equilibrium thermodynamic closures in the convective parameterization. We refer to these as quasi-equilibrium tropical circulation models (QTCMs). In particular, the model presented in NZ uses a version of the Betts and Miller (1986, 1993) deep convection scheme, in which it is assumed that the ensemble effect of deep convection is to reduce a certain measure of convective available potential energy (CAPE). This tends to constrain the large-scale temperature profile, and thus the baroclinic pressure gradients. Analytical solutions for deep convective regions based on this were produced as part of an ongoing project, summarized in Neelin (1997, hereafter N97). The QTCM makes use of these analytical solutions as basis functions within the numerical model, an approach referred to as "tailored basis functions", since the retained vertical structures are tailored to the dominant physics of interest. This provides a way of taking "quasi-equilibrium thinking" (reviewed in Emanuel 1998) into the realm of quantitative simulation.

A small hierarchy of QTCMs is anticipated, in which successively higher accuracy is obtained by retaining additional vertical structures, or embedding additional physics. In NZ the simplest QTCM is chosen that adequately simulates primary features of the tropical climatology. This is termed QTCM1 because it retains a single vertical structure for temperature and humidity.

By its derivation, it is expected to give an accurate solution in deep convective regions (compared to, say, a GCM with Betts-Miller convection). Within one radius of deformation of deep convective regions, it should remain reasonably accurate, because temperature gradients are not large. At midlatitudes it is simply a highly truncated vertical representation, roughly equivalent to a two-layer model, since the Galerkin representation is tailored to tropical vertical structures.

To accompany this representation of dynamics, a radiation package is derived (after Chou and Neelin 1996; Chou 1997) that represents the main radiative processes at an intermediate level of complexity. This includes leading cloud-radiation interaction effects, since these are important to the general circulation, and since dynamics of convection zones is of interest. Likewise, a land-surface model is presented that includes the essentials of more complex land-surface models such as the biophysical control on evapotranspiration and surface hydrology, but retains computational and diagnostic simplicity (Zeng and Neelin 1998). The QTCM thus occupies a niche intermediate between GCMs and simpler models. It is related to GCMs in having a step-by-step derivation from the primitive equations, a convective parameterization based on parcel buoyancy considerations and two-stream radiative schemes with cloud interaction, while remaining computationally efficient and simple to analyze. For instance, Zeng and Neelin (1998) and NZ discuss ways in which the moist static energy budget allows more direct access to fundamental dynamics in convection zones, especially over land regions. An example of testing the impact of a process by intervening in the model to suppress it is provided in Lin et al (1998), in which the impact of midlatitude disturbances upon intraseasonal oscillations is tested.

We provide here a sampling of the simulation for a variety of phenomena, reviewing results that are presented in more detail in NZ, ZNC and Lin et al. (1998). The model dynamical framework, the implementation of cloud prediction, shortwave and longwave radiation schemes, and the land-surface scheme are summarized in section 2. Section 3 presents, in turn, the simulated climatology, sensitivity to departures from the QE parameterization, the intraseasonal oscillation, interannual variability forced by observed SST, including El Niño-Southern Oscillation

variability, the seasonal and interannual evolution of the Southeast Asian Monsoon, and the Amazon water budget. Conclusions are provided in section 4.

2. Model Description/Implementation

2.1 Dynamics and Convection

Approximations associated with the quasi-equilibrium assumption are used to generate analytical solutions which are then used as the first basis function in a Galerkin framework. The detailed derivations starting from the primitive equations, and interpretation of the dynamics and moist convection in the model, are discussed in NZ. The major steps include: (1) a vertical structure of temperature is chosen that can match the QE profile of the Betts-Miller scheme when QE applies (although QE is not assumed to always hold); (2) using the hydrostatic equation, the choice of the temperature profile gives the vertical structure of the baroclinic pressure gradients; (3) the baroclinic and barotropic components of the pressure gradient term yield corresponding vertical structures of the horizontal velocity components; (4) nonlinear advection terms and vertical eddy viscosity terms are projected onto these velocity components; (5) a vertical structure for the vertical velocity corresponding to the baroclinic component is derived using the continuity equation; and (6) an effective moist stability applicable to deep convective regions is derived based on the vertical velocity profile and the temperature and humidity structure.

The main prognostic equations of QTCM1 are for the amplitudes of the vertical structures of temperature T_1, humidity q_1, the baroclinic component of the horizontal velocity $\mathbf{v}_1$, and the barotropic component $\mathbf{v}_0$ (the barotropic vorticity ζ_0 is the actual prognostic variable):

$$\partial_t \mathbf{v}_1 + \mathcal{D}_{V1}(\mathbf{v}_0, \mathbf{v}_1) + f\mathbf{k} \times \mathbf{v}_1 = -\kappa \nabla T_1 - \epsilon_1 \mathbf{v}_1 - \epsilon_{01}\mathbf{v}_0 \tag{2.1}$$

$$\partial_t \zeta_0 + \mathrm{curl}_z\left(\mathcal{D}_{V0}(\mathbf{v}_0, \mathbf{v}_1)\right) + \beta v_0 = -\mathrm{curl}_z(\epsilon_0 \mathbf{v}_0) - \mathrm{curl}_z(\epsilon_{10}\mathbf{v}_1) \tag{2.2}$$

$$\widehat{a}_1(\partial_t + \mathcal{D}_{T1})T_1 + M_{S1}\nabla \cdot \mathbf{v}_1 = \epsilon_c^*(q_1 - T_1) + (g/p_T)(-R_t^{\uparrow} - R_s^{\downarrow} + R_s^{\uparrow} + S_t - S_s + H) \tag{2.3}$$

$$\widehat{b}_1(\partial_t + \mathcal{D}_{q1})q_1 - M_{q1}\nabla \cdot \mathbf{v}_1 = \epsilon_c^*(T_1 - q_1) + (g/p_T)E \tag{2.4}$$

where $\mathcal{D}$ represents the projected advection and diffusion of the corresponding variables, a hat denotes vertical averaging, M_{S1} and M_{q1} are effective dry static stability and moisture stratification, ϵ denotes various effective damping/coupling coefficients, E is evaporation, H is sensible heat flux, S is shortwave flux, and R is longwave radiative flux. Note that the projections lead to terms containing vertical averages of the profiles such as $\widehat{a}_1$. The convective heating term $(q_1 - T_1)$ is a projected CAPE and ϵ_c^* is inversely proportional to the relaxation time τ_c of the Betts-Miller scheme and allows departures from QE. Outside convection zones (when CAPE is negative) ϵ_c^*=0.

An alternate prognostic equation that is very useful in analyzing model dynamics is the moist static energy equation (the sum of (2.3) and (2.4))

$$\widehat{a}_1(\partial_t + \mathcal{D}_{T1})T_1 + \widehat{b}_1(\partial_t + \mathcal{D}_{q1})q_1 + M_1\nabla\cdot\mathbf{v}_1 = (g/p_T)F^{\rm net} \tag{2.5}$$

This dominates the dynamics of convective regions, where the temperature and moisture equations alone have large canceling terms. It avoids fast, $O(\tau_c)$, time scales which go into the adjustment of CAPE. The projected moist static energy equation (2.5) is very similar to the vertically integrated moist static energy equation of the primitive equations. In both equations net flux into the column $F^{\rm net}$ balances transport by the retained degrees of freedom. Although our coding uses separate T_1 and q_1 equations, it would be possible to run the model using (2.5) and either (2.3), or a CAPE equation formed from the difference (2.3)/$\widehat{a}_1$ minus (2.4)/$\widehat{b}_1$. Within convective regions, to the extent that QE ties q_1 to T_1, (2.5) contains all thermodynamic information necessary to solve for large scales, and this can be exploited to assist in understanding results.

The vertical profiles of these prognostic variables are derived offline. The vertical profiles a_1, B_1, V_1, and V_0, as well as the profile for vertical velocity Ω_1, are shown in Fig. 1. Note that the baroclinic profile V_1 is not exactly symmetric about mid-atmospheric level as assumed in simpler models (e.g., Gill 1980), but shows more subtle structure resulting from integrating the hydrostatic equation using the retained temperature profile. Since the vertical moisture structure in moist convective regions is less constrained (see NZ), we have more freedom in choosing the

actual humidity profile b_1 such that it does not have to be the same as the fixed sub-saturation moist adiabatic profile B_1.

Given the vertical profiles, the total fields can be reconstructed at any vertical level as

$$T = T_r(p) + a_1(p)T_1(x, y, t) \tag{2.6}$$

$$q = q_r(p) + b_1(p)q_1(x, y, t) \tag{2.7}$$

$$\mathbf{v} = \mathbf{v_0}(x, y, t) + V_1(p)\mathbf{v_1}(x, y, t) \tag{2.8}$$

where T_r and q_r are the reference profiles chosen to be typical for the tropical deep convective regions, x is longitude, y is latitude, and p is pressure. Note that the model predicts the total wind while temperature and humidity are deviations from a reference profile. The reference profiles are independent of space and time, and so do not appear in differentiated terms of the equations. They are not assumed to be solutions of the equations. See NZ (appendix A) for discussion of impact of the reference profiles.

2.2 Cloud Prediction and Radiation

2.2.1 Cloud Prediction

As shown in Chou (1997), four cloud types, deep cloud, cirro-cumulus/cirro-stratus (CsCc), cirrus and stratus, as classified in the ISCCP (the International Satellite Cloud Climatology Project) data (Rossow and Schiffer 1991) can capture 80% of radiation budget in the tropics. We aim to develop parameterizations for these four cloud types in the QTCM. For the QTCM, the primary concern is to simulate mean cloudiness averaged over weekly time scale and large spatial scales, rather than to simulate cloudiness variations at every time step. We thus work with cloud cover types rather than the usual GCM level-by-level and prognostic approach. Cloud cover types have a defined vertical structure, for instance, deep convective tower accompanied by a fixed area of anvil. A single cloud type that includes the deep and anvil clouds is found to have a good linear relationship with large-scale precipitation.

2.2.2 Longwave radiation scheme

Longwave radiation is derived from a simplified longwave radiation scheme (Chou and Neelin 1996) with the Green's functions projected on the retained basis function in temperature and moisture. Because of this projection, only three components of longwave radiative fluxes, $R_t^{\downarrow}$, $R_s^{\uparrow}$ and $R_t^{\uparrow}$ are needed in the QTCM. The weakly nonlinear longwave radiation scheme coded in the packages of clrad1 and clrad1-d is

$$\begin{aligned} R_t^{\uparrow} &= R_{rt}^{\uparrow} + \sum_{n=0}^{N} \alpha_n [\epsilon_{RT_1t}^{\uparrow n} T_1 + \epsilon_{Rq_1t}^{\uparrow n} q_1 + \epsilon_{RT_st}^{\uparrow n} (T_s - T_{sr})] + \sum_{n=1}^{N} \epsilon_{R\alpha_n t}^{\uparrow} (\alpha_n - \alpha_{rn}), \\ R_s^{\downarrow} &= R_{rs}^{\downarrow} + \sum_{n=0}^{N} \alpha_n [\epsilon_{RT_1s}^{\downarrow n} T_1 + \epsilon_{Rq_1s}^{\downarrow n} q_1] + \sum_{n=1}^{N} \epsilon_{R\alpha_n s}^{\downarrow} (\alpha_n - \alpha_{rn}), \\ R_s^{\uparrow} &= R_{rs}^{\uparrow} + \epsilon_{RT_ss}^{\uparrow} (T_s - T_{sr}), \end{aligned} \tag{2.9}$$

where α_n and α_{rn} are cloud fraction and reference cloud fraction for cloud type n, and $n = 0$ represents clear sky. In (2.9), α_{rn} can be set to zero, and then $R_{rt}^{\uparrow}$ and $R_{rs}^{\downarrow}$ are the values for clear sky. Here α_{rn} is just for consistency with the linear scheme [see NZ Eq. (4.45)]. Coefficients in the scheme are pre-calculated as, for instance,

$$\epsilon_{Rq_1t}^{\uparrow n} = \int_{p_0}^{p_s} G_q^{\uparrow n}(p_t, \hat{p}) b_1(\hat{p}) d\hat{p} \tag{2.10}$$

with $G_q^{\uparrow n}$ obtained from Harshvardhan et al. (1987) scheme, a full longwave radiation scheme. This scheme is not that much more complex than a Newtonian cooling in formula but maintains the complexity of a full longwave radiation scheme in physics.

2.2.3 Shortwave radiation scheme—clrad1 and clrad1-d

Surface solar irradiance ($S_s^{\downarrow}$) and net solar absorption by the atmospheric column ($S_t^{\downarrow} - S_t^{\uparrow} - S_s^{\downarrow} + S_s^{\uparrow}$) are the primary components of shortwave radiative fluxes required in the QTCM equations during integration. The solar radiative fluxes mainly depend on solar zenith angle (θ) and surface albedo (A_s). The impact of variations of aerosol and atmospheric gases, such as ozone and CO_2, on the solar radiative fluxes are relatively small compared to the

dependence on θ and A_s. Therefore, the first order variation of the solar radiative fluxes can be approximated by simple formulas,

$$S_t^{\downarrow} - S_t^{\uparrow} - S_s^{\downarrow} + S_s^{\uparrow} = S_0 cos\theta \sum_{n=0}^{N} \alpha_n f_{an}(\theta) g_{an}(A_s), \tag{2.11}$$

$$S_s^{\downarrow} = S_0 cos\theta \sum_{n=0}^{N} \alpha_n f_{sn}^{\downarrow}(\theta) g_{sn}^{\downarrow}(A_s), \tag{2.12}$$

where S_0 is solar constant. Subscripts "a" indicate quantities associated with atmospheric absorption, and subscripts "s" indicate quantities associated with (downward) surface flux. Subscripts "n" indicate cloud type. To obtain the functions $f_{an}(\theta)$, $g_{an}(A_s)$, $f_{sn}^{\downarrow}(\theta)$ and $g_{sn}^{\downarrow}(A_s)$, we use the Fu and Liou (1993) solar radiation scheme and input a typical vertical profile of water vapor, temperature, CO_2, ozone, and aerosol. We then use curve fitting to approximate these two functions for conditions with clear sky and with different cloud types. This stripped-down shortwave radiation scheme captures the first order effects of radiative processes in the Fu and Liou scheme implicitly, for instance multiple scattering between cloud base and the surface. Surface albedo in the current QTCM is monthly climatology derived from Darnell et al. (1992) which is consistent with the ERBE (the Earth Radiation Budget Experiment) data.

2.2.4 shortwave radiation scheme—clrad0

A simpler shortwave radiation scheme is also provided for use in QTCM1. The scheme clrad0 assumes highly simplified physics, but the assumptions are more transparent. Following Kiehl (1992) and Zeng and Neelin (1998), the scheme assumes a single layer of cloud/atmosphere with a lumped reflectivity A_c (including contributions from clouds, aerosol and atmospheric backscattering) and absorptivity $a_{\rm bs}$ (including contributions from water vapor, clouds, etc.). A single cloud type combines high and middle clouds and the cloud cover is proportional to the model precipitation (section 2.2.1). Given a surface albedo A_s, one can derive the fluxes at surface and top (see Zeng and Neelin 1998 for details). For instance, the downward flux at the

surface and upward flux at the top are

$$S_s^{\downarrow} = (1 - A_c)(1 - a_{\rm bs})S_0 cos\theta \tag{2.13}$$

$$S_t^{\uparrow} = \{(1 - A_c)^2(1 - a_{\rm bs})^2 A_s + A_c\} S_0 cos\theta \tag{2.14}$$

A diurnally averaged solar zenith angle dependence has been absorbed in A_c and $a_{\rm bs}$.

2.3 Land-Surface Model

We have developed a land-surface parameterization scheme of intermediate complexity. It is much simpler than most current land-surface models (e.g., Dickinson et al. 1993, Sellers et al. (1996), but nevertheless models the first-order effects relevant to climate simulation including biophysical aspects,while from a diagnostic and computational point of view, it is only moderately more complicated than a bucket model (Manabe et al. 1965). It is termed Simple-Land, or simply SLand. It does not attempt to resolve accurately the diurnal solar and environmental control on photosynthesis. Thus the soil moisture and seasonal variation of radiation are the main controlling factors. The most essential features for climate simulation are the low heat capacity of the land surface and specification of land albedo for the surface energy budget, and soil moisture and its consequences for the surface water budget. Subgrid-scale variability of rainfall can significantly influence surface runoff and interception loss, and therefore evaporation. Various analytical formulations have been proposed (e.g., Entekhabi and Eagleson 1989). We essentially follow the same statistical approach but with choices more in line with the level of complexity of our atmospheric model.

In SLand, a single soil layer is assumed but with different depth for the energy and the water balance. For the energy balance, it essentially models the top soil layer with a typical thickness of 10cm. The prognostic equation for ground temperature T_s is:

$$C_s \frac{\partial T_s}{\partial t} = F_s^{rad} - E - H \tag{2.15}$$

Where C_s is the soil heat capacity, $F_s^{rad} = S_s^{\downarrow} - S_s^{\uparrow} + R_s^{\downarrow} - R_s^{\uparrow}$ is downward net radiation at surface, E is the total evaporation and H is the sensible heat flux. A small heat capacity C_s leads

to a damping time scale on the order of one hour, so on time scales longer than a day, one has

$$F_s^{rad} - E - H \approx 0 \tag{2.16}$$

This flux zero condition has been used explicitly by some early GCMs, and it imposes arguably the most important control on land-surface/atmosphere interaction (Zeng and Neelin 1998, NZ).

The water budget equation in a single soil layer that represents the root zone is:

$$\frac{\partial W}{\partial t} = P - E_I - R_s - E_T - R_g \tag{2.17}$$

where W is the soil moisture content per unit area and P is the precipitation, E_I is the interception loss, E_T is and the evapotranspiration, R_s is the surface runoff (the fast component) and R_g is the subsurface runoff (the slow component). The soil is saturated when W equals the field capacity W_0, which is surface-type dependent. It is useful to define a relative soil wetness

$$w = W/W_0 \tag{2.18}$$

such that w is unity at saturation.

A main objective of SLand is to model the land-surface fluxes at large spatial and long temporal scales by statistically taking into account smaller and faster scale variations. In the above parameterizations the dependent variables are w, F_s^{rad} and P. In the current version of the model, we use the following parameterizations: For interception loss:

$$E_I = E_I(P, F_s^{rad}) \tag{2.19}$$

The intercepted water is not available for surface runoff:

$$R_s = w^4(P - E_I) \tag{2.20}$$

and subsurface runoff is:

$$R_g = w^{2B+3} R_{g0} \tag{2.21}$$

where R_{g0} is the subsurface runoff at saturation and B is the Clapp-Hornberger exponent. For evapotranspiration:

$$E_T = (r_s + r_a)^{-1} \rho_a (q_{sat}(T_s) - q_a) \tag{2.22}$$

where $r_a = (C_D V_s)^{-1}$ is the aerodynamic resistance, and r_s is a bulk surface resistance including stomatal/root resistance parameterized as:

$$r_s = r_{s_{min}} w^{-\frac{1}{4}} \tag{2.23}$$

where $r_{s_{min}}$ is the minimum value of r_s occurring at no water stress ($w = 1$). The soil moisture dependences in R_s and R_g are essentially the formulations used in BATS (the Biosphere-Atmosphere Transfer Scheme, Dickinson et al. 1993). The nonlinear dependence of r_s on w takes into account effects of the soil moisture uptake by deep roots under relatively dry conditions, such as what happens during the Amazon dry season. The actual form is chosen in accordance with observations and physically based parameterizations including heterogeneity effects (e.g., Entekhabi and Eagleson 1989).

Although the scheme allows many land-surface types as long as the relevant parameter values are provided, we opt for a simple classification in the standard version with three surface types: forest, grass, and desert. The most important surface properties include surface albedo and field capacity which play critical roles in the energy and the water balance, respectively. In the standard version of QTCM1, we use prescribed surface albedo derived from satellite observations (Darnell et al. 1992), while one can easily switch to using the surface albedos linked to surface type. Sensitivity studies show discernible differences at regional scales between the two methods, but these have little impact on the global patterns. Snow hydrology is not simulated in this version, since the atmospheric model is aimed at the tropics.

2.4 Implementation

The standard version of QTCM1 includes full nonlinearities in advection, convection, and land-surface processes. Clouds associated with deep convection are predicted as one combined cloud type based on a simple precipitation/cloud-cover relationship (section 2.2). In the radiation package clrad1, the climatological monthly means of stratocumulus and cirrus clouds are prescribed from observations, while the tropical mean of middle clouds are used (constant in space and time). In the simpler package clrad0, the tropical mean of low clouds is used while high

and middle clouds are predicted as one lumped cloud type according to the model precipitation. No cloud data is input for clrad0 runs. The linearized longwave radiation scheme is used in clrad0 while clrad1 uses the weakly nonlinear version. Sensitivity studies show some differences between the two packages but the overall behaviors are similar. The radiation packages are used with diurnally averaged incoming solar radiation, although diurnal cycle can be included as an option. The topographic effects on the barotropic vorticity equation are turned off in the standard version. Depending on the target phenomenon under study, one may wish to use different options, e.g., the radiation package option. The coding of the model is modularized and sufficiently transparent that this is relatively easy. An example where temperature advection is "frozen" at climatological values in order to study midlatitude-tropical interaction is given in Lin et al. (1998).

The surface fluxes are parameterized using the bulk transfer formulae following Deardorff (1972). These include momentum flux (stress) τ_s, evaporation E and sensible heat flux H. Since the current version of the QTCM lacks an explicit boundary layer, the wind speed in the bulk transfer formulae is reduced by a factor η. This mimics an extrapolation from the free atmosphere into the boundary layer based on empirical relationships.

The model domain covers the whole tropics in longitude and extends to 60° N and 60° S in latitude. A sponge boundary is applied outside 45° latitude. A horizontal resolution of 5.625° by 3.75° is used here. Selected results from the following sections have been tested at doubled resolution (in both latitude and longitude), without major changes. The prognostic equations are finite-differenced on an Arakawa-C grid (e.g., Arakawa 1998a). The baroclinic component is similar to a shallow-water equation and is solved by applying a forward-backward scheme using the updated variables immediately. The barotropic component is solved in a vorticity/stream-function formulation using an Adams-Bashforth scheme. The numerical CFL instability criterion limits the model time-step at about 20 minutes, mostly due to the momentum advection associated with midlatitude baroclinic waves. On a Sun/Ultra2 workstation, it takes less than 5 minutes CPU time per year of simulation.

3. Model Results

3.1 Climatology

Results presented in this section come from two types of runs that differ only in the boundary condition of prescribed SST: (i) 1982-1998 runs driven by the observed SST of Reynolds and Smith (1994), and diurnally averaged solar radiation at top. The latter is most relevant to the land regions. Monthly mean output from these runs is used to analyze the climatology and interannual variability. Because these runs are similar to GCM runs conducted in the Atmospheric Model Intercomparison Project (AMIP) we refer to them as AMIP-like runs; (ii) seasonal runs driven by climatological SST and diurnally averaged solar radiation. Daily mean output is used in the analyses of intraseasonal oscillation. The cloud-radiation package clrad0 is used in the runs.

The presence of temperature advection and the baroclinic and barotropic wind components in velocity (similar to a two-layer model in terms of degrees of freedom) leads to baroclinic instability and generates midlatitude storms. The "tails" of storms penetrate into the tropical convergence zones and can contribute to tropical variance. These connections tend to occur at preferred locations and this effect appears to play a role in forming the climatological southern convergence zones (Fig. 2), namely, the South Pacific Convergence Zone (SPCZ), the South Atlantic Convergence Zone (SACZ), and a similar feature in the South Indian Ocean. In observations, these southeastward extensions of the convergence zones are generally quite broad whereas the model appears to have narrower versions of these. The storms play an important role in drying the subtropics and feeding the moisture to midlatitudes. The storms appear to organize themselves somewhat in the North Pacific and North Atlantic, albeit not at realistic locations, likely due to the lack of topographic effects. However, the poleward edges of the subtropical dry zones are a little too wide, and the storms are too far poleward. The subtropical high pressure regions such as in the southeastern Pacific appear to be slightly too dry, and extend too far east such that southern South America is too dry. This is also partly responsible for the narrowness of the southeastern extensions of the convergence zones discussed above. For a model of this level of

complexity aimed at tropical climate simulation, we do not expect a perfect simulation of midlatitude storms. Major effects relevant to the tropics are the eddy flux of moisture, which dries the subtropics, and the eddy flux of momentum, which maintains the tropical zonal mean easterlies as discussed in NZ. The link between the subtropical and tropical convergence zones also appears relevant to teleconnections of climate anomalies. We now shift our attention to the seasonal cycle of the rainfall patterns (Fig. 2).

In January, the major convective band runs over most of the equatorial tropics, including the western Pacific warm pool region, the Amazon, Central Africa, and the Indian Ocean. However, parts of the ITCZ in the eastern Pacific and Atlantic are too weak. Sensitivity studies show that these features are sensitive to the parameterization of surface fluxes. The present version also lacks a separate explicit boundary layer which is thought to be important in maintaining the strength of these narrow convergence zones (Wang and Li 1993). As the sun moves northward, the equatorial convergence band also moves northward from January to July. The ITCZ over the eastern Pacific and the Atlantic strengthens. Many detailed features are also captured by the model, such as the dry region in Northeast Brazil between the ITCZ and SACZ, the wet region around Madagascar, and the mid-Pacific trough near Hawaii. Throughout a seasonal cycle, rainfall over the Amazon basin is reasonable, but rainfall over Africa appears to be too strong all year round.

In July (Fig. 2b), the African and North American monsoons are well established. The largely zonal monsoon rain in West Africa extends from the rainforest into the Sahel at about 15N. A wet tongue extends from Central America along the Pacific coast into Mexico and Southwest US. The patterns and locations are quite similar to the observations (not shown). The Asian monsoon region, India, Southeast and East Asia receive large amount of monsoon rainfall. However, the Asian monsoon appears to be too weak, especially in contrast with the unrealistically large maximum rainfall sitting over equatorial Indian ocean. A maximum over the Bay of Bengal is missing in the model. Another unrealistic feature is a large maximum around the dateline. A similar tendency has been noted in some runs of the UCLA AGCM (R. Mechoso,

personal communication). This is found to be sensitive to the evaporation parameterization (ZNC).

Overall, the model simulates a reasonable seasonal migration of tropical and subtropical convective rainfall centers. The African and American monsoons are well simulated, but the rainfall over the Indian ocean and Pacific ocean is concentrated too much along the equator. Correspondingly the Asian monsoon appears somewhat weak. This suggests that the warmed continent in the model is able to shift the overall circulation, but not enough in the case of the Asian monsoon where other factors such as topography also play important role.

We now examine various other fields. Figure 3 depicts the January climatology of evaporation, OLR (Outgoing Longwave Radiation), and net downward energy flux at surface. These fields are representative of the behavior of the model's physics packages, especially surface fluxes, cloud and radiation. Over the tropical oceans, the evaporation (Fig. 3a) pattern is determined mostly by SST and surface wind speed. The SST dependence is seen in the contrast between, say, the western Pacific warm pool and the cold tongue region. The wind speed dependence is apparent in the trade wind regions such as North and South Pacific in the subtropics. Similar to the observations, the warm pool also has a local minimum due to the weak winds there. Experiments show that the evaporation in weak wind region depends critically on the minimum wind in the evaporation formula which represents sub-Reynolds scale wind variability. The overall pattern and magnitude of evaporation are similar to the observations. Over land, the evaporation tends to follow precipitation but lasts longer into the dry season due to the soil moisture memory so that the pattern of evaporation is generally smoother than that of precipitation.

The model captures the pattern of low OLR (Fig. 3b) associated with tropical convergence zones due to the longwave trapping effects of the deep convective clouds, which are predicted according to precipitation in the model. Minimum values of near 200 W m^{-2} are seen in the warm pool region and over the Amazon. As in the observations, the OLR increases toward the dry subtropics, and decreases again at midlatitudes due to the presence of clouds and colder

temperature. The OLR is slightly high, partly due to a dry bias resulting in not enough greenhouse trapping.

The net surface flux F_s (Fig. 3c) is the sum of the net radiation, evaporation and the sensible heat flux. It is nearly zero over land at climate scales due to the low heat capacity of land (section 2.3). Over ocean this quantity is important for coupling to ocean models. The simulated pattern is largely similar to the observations (not shown), exhibiting a gross seasonal contrast between the two hemispheres. In the tropics, this gradient is significantly modified by the circulation patterns. The SPCZ has a strong signature as can be seen by tracing, say, the 50 W m^{-2} contour line. The warm pool region has nearly zero net flux, similar to the observations. Near the eastern side of the ocean basins, F_s is overestimated because of the lack of stratus clouds. The fluxes under the storm tracks are captured, but somewhat underestimated.

Figure 4 depicts the model 850mb and 300mb winds [reconstructed using (2.8)]. At 850mb, the model simulates trade winds blowing across the subtropics. The trades are especially strong in the winter Northern Hemisphere. Midlatitude westerlies develop associated with the storms. The anticyclonic motions around the subtropical highs are well simulated, especially in the Southern Hemisphere. The winds turn southeastward correctly over the Amazon Basin despite the lack of topography, suggesting that this is mostly a thermodynamical feature rather than a topographic one. Equatorial westerlies are also seen over Africa and the Indonesian region, although they are not strong enough over the Indian Ocean. The 300mb (Fig. 4b) winds are dominated by the subtropical westerly jets. The northern Hemisphere jet is located at about 30N, similar to observations, but the southern hemisphere jet is somewhat too close to the equator. Both jets are slightly too strong. The tropics are dominated by the easterlies with a hint of change to westerlies in the so-called westerly duct region in the Eastern Pacific, although not as strongly westerly as in the observations.

Figure 5 shows the zonal average zonal velocity. The northern Hemisphere trades are centered at about 15N, similar to the observations. The subtropical jets are somewhat too strong, and the easterlies extend slightly too far poleward. These correspond to a slightly too high wind

shear at midlatitudes in the baroclinic mode which is derived from a tropical moist adiabat profile by design. Overall, given the limited degrees of freedom, the model simulated wind field is quite encouraging.

The July climatology of the atmospheric temperature averaged between 500mb and 200mb [reconstructed using (2.6)], surface temperature, soil wetness and 850mb wind are shown in Fig. 6. The atmospheric temperature at 500-200mb is chosen so that a direct comparison with the observation of Li and Yanai (1996, their figure 3) can be made. The most prominent feature in Fig. 6a is the warm temperature center around Tibetan Plateau, corresponding to high pressure aloft and low pressure at low levels for the baroclinic component. Careful examination indicates that this monsoon depression is located slightly too far west of the Tibetan Plateau (which does not exist in this model run). At 850mb, the southwesterly winds over the Indian Ocean turn around this monsoon depression and then join the trade winds from the western Pacific, flowing northward into the Eastern Asian trough (Fig. 6d). Over North America, a temperature ridge has developed associated with the North American monsoon.

3.2 How much do departures from quasi-equilibrium affect climatology?

A model run was conducted with a convective adjustment time τ_c (related to ϵ_c^* in (2.3) and (2.4); NZ) of 8 hours rather than 2 hours as used in the control run. The January precipitation is shown in Fig. 7. Compared to the control case (Fig. 2a), the tropical convergence zones appear to be slightly weaker, especially the eastern Pacific ITCZ. However, they are very similar to each other overall. This low sensitivity to τ_c is comforting because in the real tropical atmosphere, the adjustment time might vary significantly due to mesoscale organization and other disturbances. This insensitivity is rooted in the enthalpy constraint (latent heating comes from water vapor condensation) so that the adjustment time does not enter the moist static energy equation (2.5) which tends to determine the large-scale circulation patterns (NZ sections 5.2, 7). However, this finite relaxation time can have non-negligible impact on waves of faster time scale (N97).

3.3 Intraseasonal Oscillation

The model lacks mesoscale organization in the tropics and is relatively steady compared to storm-related variations in midlatitudes. Nonetheless, it does exhibit a significant amount of intraseasonal variability. Figure 8 is a time-longitude plot showing 850mb winds on equator over a year. An eastward propagating Madden-Julian oscillation (MJO)-like signal is apparent, though the amplitude is somewhat weak. The amplitude and phase speed vary both seasonally and between events, and are sensitive to various parameters including the evaporation formulation. Spectral analysis (Fig. 9a) indicates a broad peak around 30 days at wave number 1. Significant spectral peaks are also found for wavenumbers 2 and 3 (Lin et al. 1998).

In order to study the mechanisms of the excitation and maintenance of the model intraseasonal oscillation, experiments with an earlier version of the model (beta-version) were conducted to examine the effects of the evaporation-wind feedback (EWF, Emanuel 1987, Neelin et al. 1987) and midlatitude disturbances. The following cases are simulated: (1) a control run, using the standard version of QTCM1 V1.0, with evaporation-wind feedback and extratropical disturbances included, (2) evaporation-wind feedback turned off, (3) extratropical disturbances turned off by using the mean temperature advection from a previous run, (4) both the EWF and extratropical disturbances turned off. The corresponding spectra are shown in Fig. 9. The lack of EWF significantly reduces the amplitude of variances in spectral band associated the model MJO (Fig. 9b). Variances remains, and is even enhanced at lower frequencies. The most dramatic impact occurs in the case where extratropical disturbances are suppressed. The peak in the 850 mb wind spectra is almost completely eliminated (Fig. 9c). The experiments suggest that both the EWF and extratropical excitation act to maintain the MJO. If either of the mechanisms is removed, the MJO-like oscillation is reduced. Of the two mechanisms, the removal of extratropical excitation decreases the amplitude of the oscillation more than removing the EWF.

3.4 Interannual Variability

The AMIP-like runs with observed SST permit examination of the model simulated climate variability on interannual time scales. Figure 10 shows the precipitation on the equator from the model during January 1982 to March 1998. The model captures the major El Niño warm events of 1982-83, 86-87, 91-92, and 97-98 which have anomalies extending all the way across the eastern Pacific, as well as the long-lasting warming events in the first half of the 1990s. The cold La Niña events of 1984, 88-89, 95-96 are also captured. During 1986-87 and 91-92, the modeled rainfall anomalies in the eastern Pacific are not as strong as in observations, although the eastward extension in 1982-83 and 97-98 is reasonable. The maxima around the dateline are often too large during the summer. Our sensitivity studies suggest that these are both related to deficiencies in climatology, namely, the weak ITCZ and the maximum around the dateline in summer (see discussion in section 3.1). An annual modulation of the longer warm or cold events can be seen clearly around the dateline, again an indication of the anomaly dependence on the climatology. This annual modulation is also seen in observations although it is noisier. In addition to rainfall increases directly associated with warm SST during El Niño, the model also captures several aspects of the rainfall reductions in the western Pacific/Indonesian region, and vice versa during La Niña. Over South America and the Atlantic, the correspondence in magnitude and seasonal timing of anomalies is imperfect but the model produces counterparts to several of the major anomalies, e.g., in 1984, 87, 88, 91-92, 96 and 97. A significant success is the the longitudinal position of the ENSO anomalies, and the variation of the extent and position of these anomalies during the larger El Niños of 1982-83 and 1997-98. Simple models often have difficulty with these aspects, and the dynamics involves the nonlinear simulation of the convecting/nonconvecting boundary.

In order to see the spatial pattern of the interannual variability, we plot in Fig. 11 a composite winter precipitation difference between three El Niño years (1986-87, 91-92, 94-95) and three La Niña years (1983-84, 88-89, 95-96; warm events minus cold events). The main positive

precipitation anomaly is centered just east of the dateline, showing changes in the ITCZ and SPCZ. The model's positive anomaly does not extend quite as far west along the equator as the observations. Surrounding this are negative anomalies over the Indonesian region, subtropical south and north Pacific. Further away, reduced precipitation is seen over the Amazon and northeastern Australia. In general the model captures these observed teleconnection patterns, although some details are questionable. Interestingly, some teleconnections to subtropical latitudes are also present, including over southeastern Africa, the enhanced SACZ over southeastern Brazil, and a hint of a positive anomaly along the California coast, although the latter two are hard to see at this contour interval. These presumably involve Rossby wave dynamics (Wallace and Gutzler 1981), but, at least in the southern hemisphere, involve interactions with the convective zones, so may be more complex than simple external mode Rossby waves.

The mature phase of the monsoons has been discussed in section 3.1. We now wish to take a closer look at its interannual variability. The monsoons have strong interannual variability and this variability is not in general satisfactorily simulated in GCMs with interannual SST forcing (Sperber and Palmer 1996). It is of great interest to see how the QTCM, a much simpler model but nevertheless with the main physics included, simulates this. In doing so, a practical difficulty is the lack of a universally accepted monsoon index. Here we choose the Asian monsoon wind shear index (zonal velocity at 850mb minus 500mb in the region 0-20N, 40-110E) of Webster and Yang (1992). This is a natural index for the present model because it is simply proportional to the strength of the baroclinic component (the barotropic component has constant velocity in the vertical, Fig. 1), which is driven directly by horizontal gradients in the thermodynamics.

An ensemble of 10 model runs that differ only in the initial condition are analyzed. Figure 12 depicts interannual variation of the model simulated Asian monsoon wind shear index averaged for June, July and August of each year. Unlike most GCMs (Sperber and Palmer 1996), the present model shows variation among the 10 ensemble runs of less than 0.5 m s^{-1} while the range of interannual variation of this index is about 5 m s^{-1}. This lack of variation among

ensemble runs is likely due to omission of some processes responsible for some types of atmospheric internal variability. On the other hand, this lack of "noise" can be an advantage for analysis of the processes and mechanisms the model does represent.

Because the observations contain a significant amount of atmospheric internal variability that is not reproducible, it is not clear to what extent agreement between models forced by SST and observations is expected. The general level of agreement between the QTCM and the observations is similar to what has been found for the GCM simulations in the AMIP project (Sperber and Palmer 1996). The results show a tendency toward negative correlation with ENSO. For instance, the warm El Niño events in the summers of 1983, 87, 97 correspond to weak monsoon by the wind shear index. The relation with the cold phases is less clear. In 1989 an increase is noted in both model and observations, but this does not hold well in other La Niña years. Since the model does not simulate snow hydrology (section 2.3), this level of agreement suggests that the SST may play a more important role in the interannual variability of large-scale monsoon.

The strong hydrological cycle in the Amazon Basin, with a rainfall rate of over 2000mm a year, provides an excellent testbed for the land-surface model and the convective dynamics. Fig. 13 shows the 12 month running means of various components of the hydrologic cycle. A negative correlation with ENSO is clearly seen in precipitation, runoff and soil moisture content while evaporation varies only slightly for the reasons discussed in section 3.1. These trends are found also in observations (e.g., Zeng 1998), although details of magnitude can differ. For instance, the 1988-1989 La Niña event leads to an increase of about one mm day^{-1} in precipitation and a corresponding increase in soil water storage. A delay on interannual time scales in soil moisture and runoff from precipitation is also noticeable. This memory effect might play a role in season-to-season climate anomalies and act as a link between climate variation in the Pacific and Atlantic. The atmosphere and land-surface models developed here thus provide an efficient tool for studying this type of problem.

4. Conclusion

QTCM1 aims to simulate reasonably complex tropical phenomena with a relatively streamlined tool. A unique feature is that aspects of the dominant sub-grid scale processes, namely moist convective dynamics, are employed in the model design. In this approach, we benefit from two strands of work pioneered by Akio Arakawa: QE convective parameterization and numerical modeling of the atmosphere. We attempt to use constraints provided by the first to produce shortcuts in the latter, at least for specific aspects of simulation of the general circulation. In terms of the boxes in Fig. 18 of Arakawa (1998b), we provide a tool that explicitly bootstraps solution of the "dynamical processes" by making use of properties of the "cloud processes". In doing so, the links between the two become clearer, consistent with the theoretical approach of "QE thinking" discussed in Emanuel (1998). In this paper, we present a sample of results from the first QTCM.

The tropical climatology simulated by QTCM1 appears reasonable, showing the seasonal migration of the tropical convective zones and the variation of the trades. The African and American monsoons are well represented, but the Asian monsoon is somewhat too weak. For a model with only two degrees of freedom in the vertical (a baroclinic and a barotropic component), the reconstructed wind fields are quite decent; the good accuracy despite the high truncation indicates that the effort spent on the analytical solution prior to turning to numerical methods (see NZ) was well invested. The model does a reasonable job in simulating fields such as surface evaporation, OLR, and net surface energy flux that are representative of the model physical parameterizations. These fields are of importance to coupled ocean-atmosphere modeling and are not usually simulated in simple models.

A multi-year model run driven by the observed SST anomaly from 1982 to 1998 demonstrates the model's ability to simulate the atmospheric interannual response in precipitation and other key fields. The primary ENSO rainfall anomalies are simulated near the dateline, extending further eastward during large warm events. Also simulated are the reduced

rainfall regions in the tropical western Pacific/Indonesian region, and South America. Certain subtropical teleconnections are also captured. For instance, the Amazon hydrologic cycle exhibits a correlation with ENSO. Differing teleconnection mechanisms over land and ocean regions in response to ENSO anomalies are noted. These involve feedbacks from moist convection, cloud radiative effects and land-surface processes, as will be described elsewhere.

The model monsoon wind shear index as defined by Webster and Yang (1992) shows significant interannual variability and some correlation with ENSO warm events. The behavior and level of agreement with observations are similar to those of GCMs in the AMIP project. This suggests a significant role of SST variations in influencing the land-sea thermal contrast, with feedbacks from land processes.

Having originally derived the model framework with theoretical applications in mind, the quantitative simulation presented here can be viewed with some satisfaction. Although we did not expect it from a model of this complexity, the simulation of certain fields is quite comparable with that of many GCMs at similar resolution. The climatology of tropical precipitation, for instance, while imperfect with respect to observations, appears to be better than that of several GCMs of the previous generation, including the GFDL R15 model as analyzed in Lau (1985), the older UCLA GCM version (Mechoso et al. 1987), and the older versions of the community climate model CCM1 and CCM2 (Hurrell et al. 1993). These GCMs have proven their worth in many studies, so the comparison is encouraging. Comparison to more recent GCM versions is left to the reader. In comparing with GCMs, it is understood that the problem solved is less complex in several respects. The point made here is simply that QTCM1 can be used to reproduce certain types of results studied in GCMs but within a system that is much more accessible to theoretical analysis.

In developing the model, including the cloud-radiative parameterizations and land-surface model, we were always aware of the parallel with earlier work carried out in GCMs, including Arakawa's experience with the early two-layer UCLA GCM (Arakawa 1998a). Have we merely revamped a two-layer GCM in Galerkin form? Some important differences include: an underlying

analytical solution of the primitive equations plus deep convective parameterization that holds under certain conditions; a connection to parcel buoyancy considerations in the convective parameterization by reduction of CAPE, even in the projected system; more general vertical structures, including for cloud types, than are normally admitted in level or layer models; and formulation and parameterizations that are designed to be reducible into even simpler versions for analysis. The model also contains an underlying physical hypothesis about the dominant effects in the tropical general circulation, as reviewed in more detail in N97. The effect of deep convection in communicating surface warming through the troposphere is seen via the effect upon pressure gradients of pulling temperature toward a moist convective profile. Column energy and moisture budgets, together forming the moist static energy budget, are important in setting the degree to which dynamics can flatten out these pressure gradients. The reasonable success of the model in quantitative simulation of many of the major tropical climate phenomena is suggestive that QE thinking is not only a powerful concept, but can also be a basis for the development of models to simulate complex tropical climate and variability.

Acknowledgments. This review is condensed from manuscript versions of Neelin and Zeng (1998), Zeng et al. (1998) and Lin et al. (1998), and was presented by the lead authors as an invited talk and poster at the Symposium on General Circulation Model Development: Past, Present, and Future, held at UCLA, January 20-22, 1998. Conversations with A. Adcroft, A. Arakawa, C. Bretherton, C. Cassou, R. Dickinson, P. Dirmeyer, K. Emanuel, R. Koster, K.-N. Liou, C. R. Mechoso, C. Perigaud, D. A. Randall, R. Seager, J. Shuttleworth, P. Webster, W. Weibel, M. Yanai, J.-Y. Yu, and S. Zebiak during the course of the project were helpful. This work was supported in part by National Science Foundation grant ATM-9521389 and National Oceanographic and Atmospheric Administration grant NA46GP0244.

References

Arakawa, A. (1993). Closure assumptions in the cumulus parameterization problem. In *The Representation of Cumulus Convection in Numerical Models of the Atmosphere*, K. A. Emanuel and D. J. Raymond, eds., American Meteorological Society.

Arakawa, A. (1998a). A personal perspective on the early years of general circulation modeling at UCLA. In *General circulation Modeling: Past, Present, and Future*. D. A. Randall, ed., Academic Press, this volume.

Arakawa, A. (1998b). Future development of general circulation models. In *General circulation Modeling: Past, Present, and Future*. D. A. Randall, ed., Academic Press, this volume.

Arakawa, A., and W. H. Schubert (1974). Interaction of a cumulus cloud ensemble with the large-scale environment, Part I. *J. Atmos. Sci.*, **31**, 674-701.

Betts, A. K., and M. J. Miller (1986). A new convective adjustment scheme. Part II: Single column tests using GATE wave, BOMEX, ATEX and arctic air-mass data sets. *Quart. J. Roy. Meteor. Soc.*, **112**, 693-709.

Betts, A. K., and M. J. Miller (1993). The Betts-Miller scheme. Chapter 9 in *The Representation of Cumulus Convection in Numerical Models of the Atmosphere.* (K. A. Emanuel and D. J. Raymond, eds.,) *Amer. Meteor. Soc., Meteor. Mon.* **24** No. 46, 107-121.

Chou, C. (1997). Simplified radiation and convection treatments for large-scale tropical atmospheric modeling. Ph. D. dissertation, University of California, Los Angeles, CA 90095, 215pp.

Chou, C. and J. D. Neelin (1996). Linearization of a longwave radiation scheme for intermediate tropical atmospheric models. *J. Geophys. Res.* **101**, 15129-15145.

Darnell, W. L., W. F. Staylor, S. K. Gupta, N. A. Ritchey, and A. C. Wilber (1992). Seasonal variation of surface radiation budget derived from international satellite cloud climatology project C1 data. *J. Geophys. Res.* **97**, 15741-15760.

Deardorff, J. W. (1972). Parameterization of the planetary boundary layer for use in general circulation models. *Mon. Wea. Rev.*, **100**, 93–106.

Dickinson, R. E., A. Henderson-Sellers, P. J. Kennedy, and M. Wilson (1986). Biosphere-Atmosphere Transfer Scheme (BATS) for the NCAR Community Climate Model. NCAR *Tech. Note TN-275+STR*, NCAR, Boulder, CO.

Emanuel, K. A. (1987). An air-sea interaction model of intraseasonal oscillations in the tropics. *J. Atmos. Sci.,* **44,** 2324-2340.

Emanuel, K. A. (1998). Quasi-equilibrium Thinking. In *General circulation Modeling: Past, Present, and Future*. D. A. Randall, ed., Academic Press, this volume.

Emanuel, K. A., J. D. Neelin and C. S. Bretherton (1994). On large-scale circulations in convecting atmospheres. *Quart. J. Roy. Meteor. Soc.*, **120**, 1111–1143.

Entekhabi, D., and P. S. Eagleson (1989). Land surface hydrology parameterization for atmospheric general circulation models including subgrid scale spatial variability. *J. Climate*, **2**, 816–831.

Fu, Q., and K. N. Liou (1993). Parameterization of the radiative properties of cirrus clouds. *J. Atmos. Sci.* **50**, 2008-2025.

Gill, A. E. (1980). Some simple solutions for heat induced tropical circulation. *Quart. J. Roy. Meteor. Soc.* **106**, 447–462.

Harshvardhan, R. Davies, D. A. Randall and T. G. Corsetti (1987). A fast radiation parameterization for general circulation models. *J. Geophys. Res.*, **92**, 1009-1016.

Hurrell, J. W., J. J. Hack, and D. P. Baumhefner (1993). Comparison of NCAR Community Climate Model (CCM) climates. NCAR *Tech. Note TN-395+STR*, 335 pp., NCAR, Boulder, CO.

Kiehl, J. T. (1992). Atmospheric general circulation modeling. In *Climate System Modeling*, Trenberth, K. E. (Ed.), Cambridge University Press, 319-370.

Lau, N.-C. (1985). Modeling the seasonal dependence of the atmospheric response to observed El Niños in 1962-76. *Mon. Wea. Rev.*, **113**, 1970-1996.

Li, C., and M. Yanai (1996). The onset and interannual variability of the Asian summer monsoon in relation to land-sea thermal contrast. *J. Climate*, **9**, 358–375.

Lin, J. W.-B., J. D. Neelin, and N. Zeng (1998). Maintenance of tropical intraseasonal variability: impact of midlatitude storms. *J. Atmos. Sci.*, Submitted.

Manabe, S., J. Smagorinsky and R. F. Strickler (1965). Simulated climatology of a general circulation model with a hydrological cycle. *Mon. Wea. Rev.,* **93,** 769-798.

Mechoso, C. R., A. Kitoh, S. Moorthi, and A. Arakawa (1987). Numerical simulations of the atmospheric response to a sea surface temperature anomaly over the equatorial eastern Pacific ocean. *Mon. Wea. Rev.*, **115**, 2936-2956.

Neelin, J. D. (1997). Implications of convective quasi-equilibrium for the large-scale flow. In *The physics and parameterization of moist atmospheric convection.* R. K. Smith, ed., Kluwer Academic Publishers, Dortrecht, The Netherlands, pp. 413-446.

Neelin, J. D., and N. Zeng (1998). The first quasi-equilibrium tropical circulation model–formulation. *J. Atmos. Sci.*, submitted.

Reynolds, R. W., and T. M. Smith (1994). Improved global sea surface temperature analyses using optimum interpolation. *J. Climate*, **7**, 929–948.

Rossow, W. B., and R. A. Schiffer (1991). ISCCP cloud data products. *Bull. Amer. Meteor. Soc.*, **72**, 2-20.

Sellers, P. J., and coauthors (1996). A revised land surface parameterization (SiB2) for atmospheric GCMs. Part I: model formulation. *J. Climate*, **9**, 676–705.

Sperber, K. R., and T. N. Palmer (1996). Interannual tropical rainfall variability in General Circulation Model simulations associated with the Atmospheric Model Intercomparison Project. *J. Climate*, **9**, 2727—2750.

Wallace, J. M., and D. S. Gutzler (1981). Teleconnections in the potential height field during the Northern Hemisphere winter. *Mon. Wea. Rev.*, **109**, 784–812.

Wang, B., and T. Li (1993). A simple tropical atmospheric model of relevance to short-term climate variation. *J. Atmos. Sci.*, **50**, 260–284.

Zeng, N. (1998). Seasonal cycle and interannual variability in the Amazon hydrologic cycle. *J. Geophys. Res.*, submitted.

Zeng, N., and J. D. Neelin (1998). A land-atmosphere interaction theory for the tropical deforestation problem. *J. Climate*, accepted.

Zeng, N., J. D. Neelin, and C. Chou (1998). The first quasi-equilibrium tropical circulation model–implementation and simulation. *J. Atmos. Sci.*, submitted.

FIGURE CAPTIONS

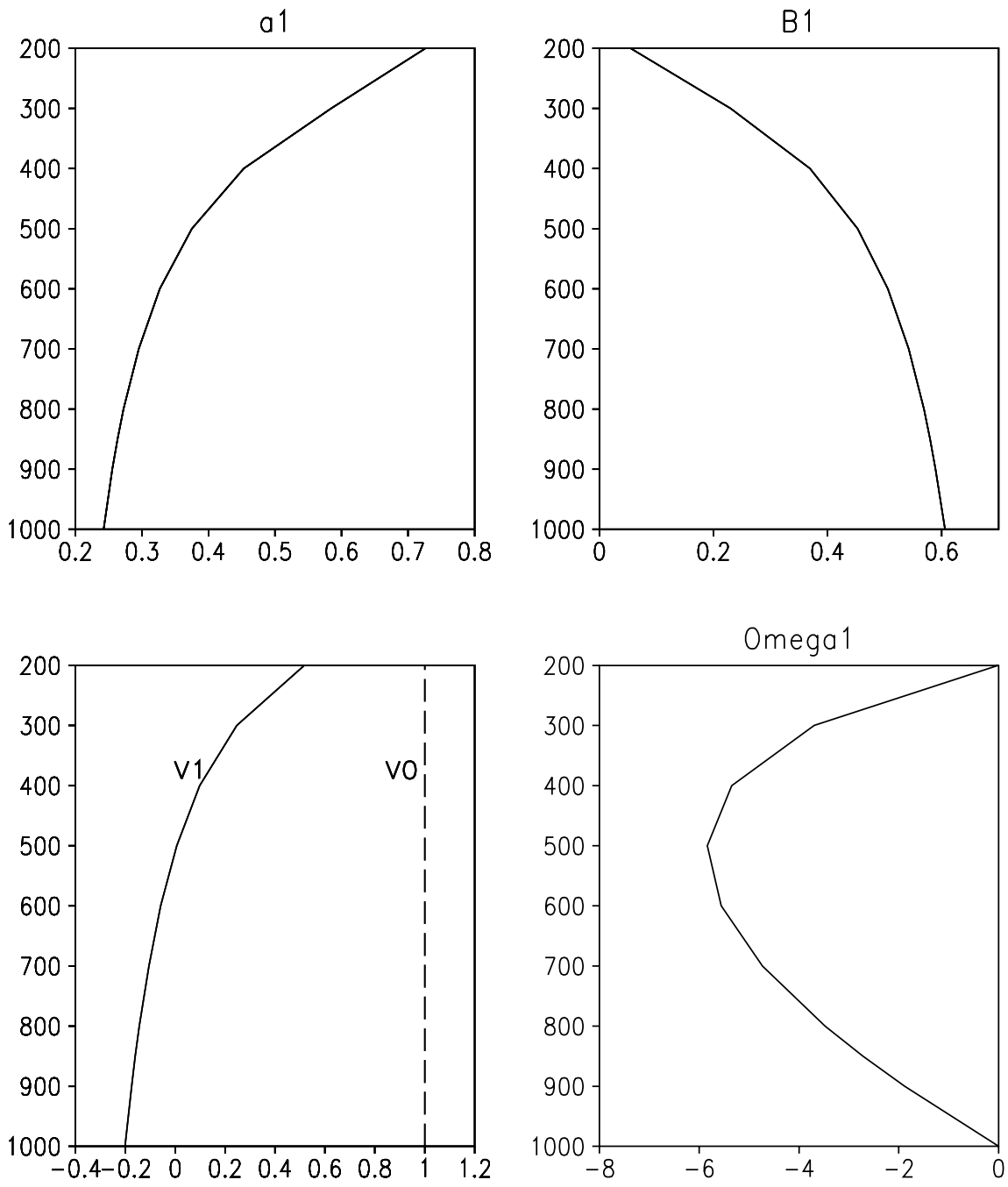

Figure 1: Vertical profiles of basis functions for (a) temperature a_1; (b) humidity B_1; (c) horizontal velocity V_1 and V_0; and (d) implied profile of vertical velocity Ω_1.

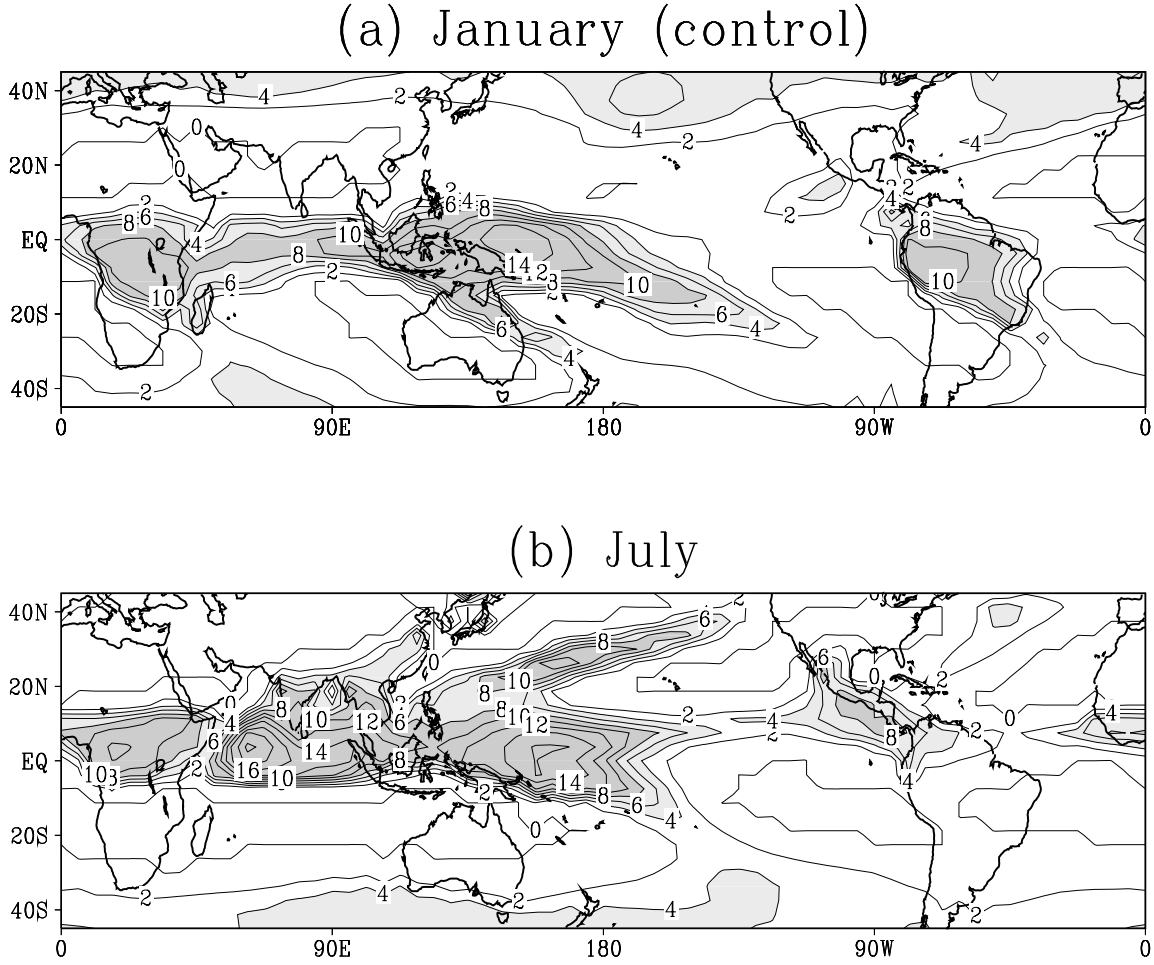

Figure 2: Model climatological monthly mean precipitation for the period 1982-1998. (a) January, (b) July. Contour interval 2 mm day^{-1}; shaded above 4 mm day^{-1}.

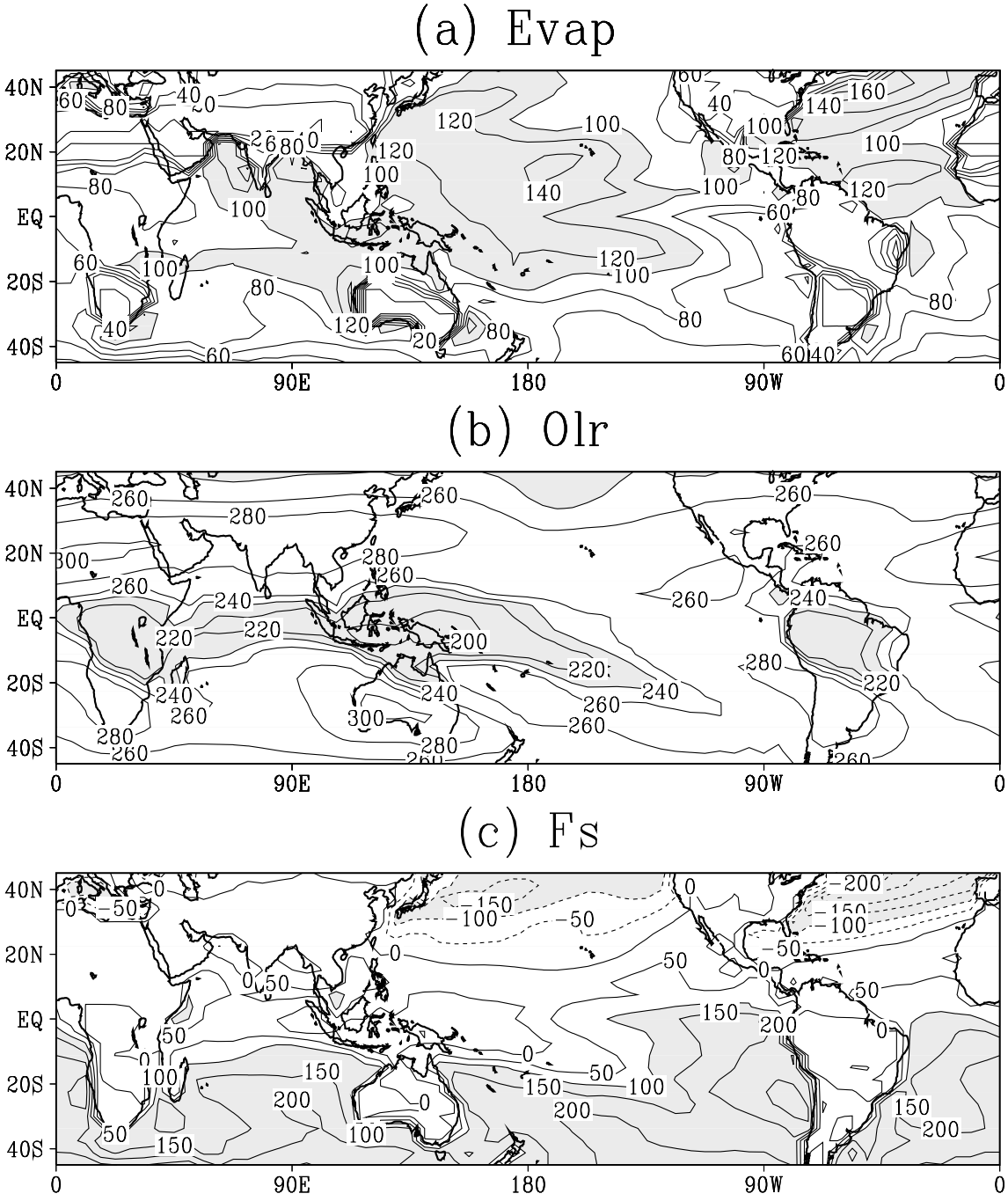

Figure 3: Model simulated January fluxes of (a) evaporation, contour interval 20 W m^{-2}, shaded above 100; (b) outgoing longwave radiation, contour interval 20 W m^{-2}, shaded below 240; (c) downward net surface energy flux $F_s^{\rm net}$, contour interval 50 W m^{-2} with dark shading above 100 and light shading below -100.

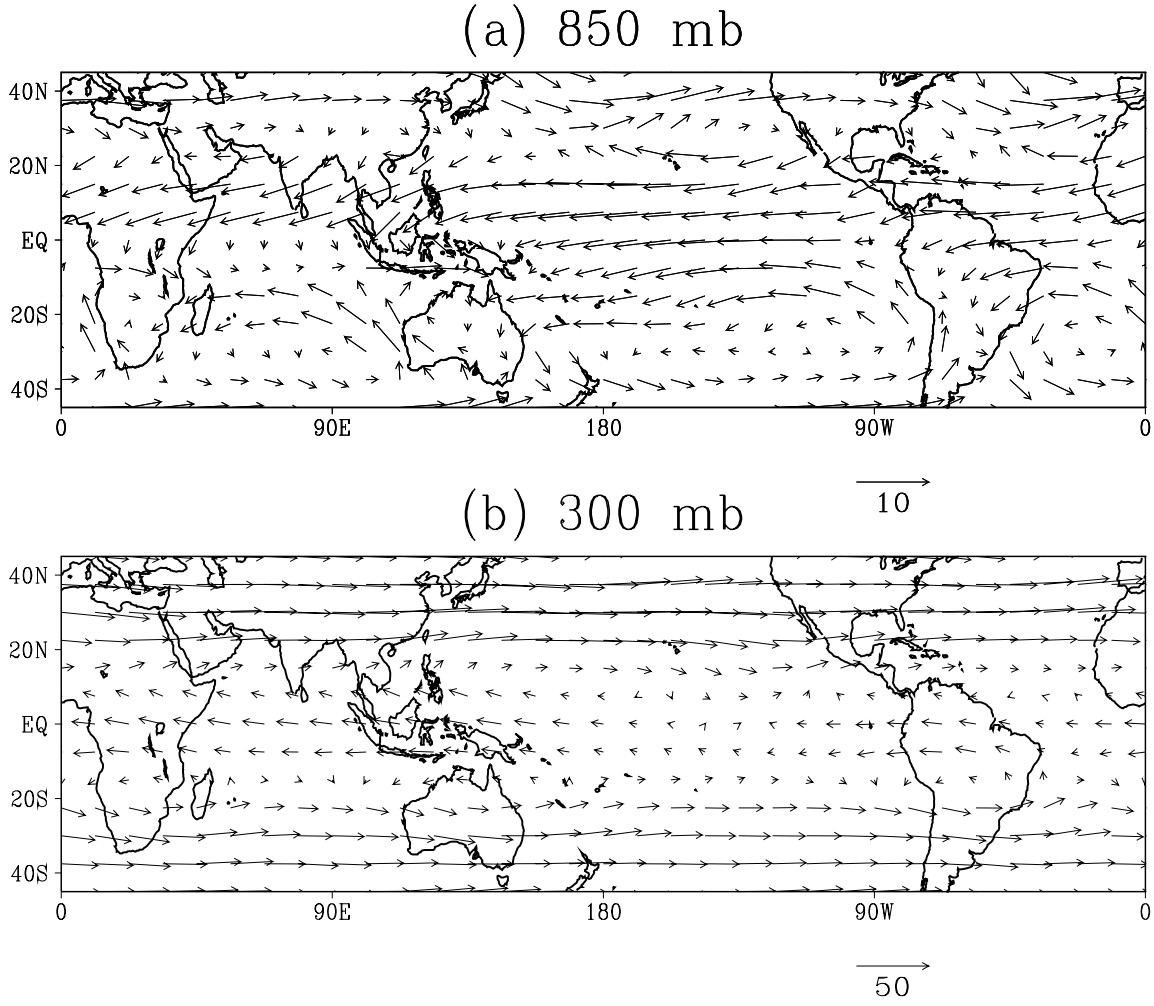

Figure 4: Model simulated January climatological winds at (a) 850mb, (b) 300mb. In m s^{-1}.

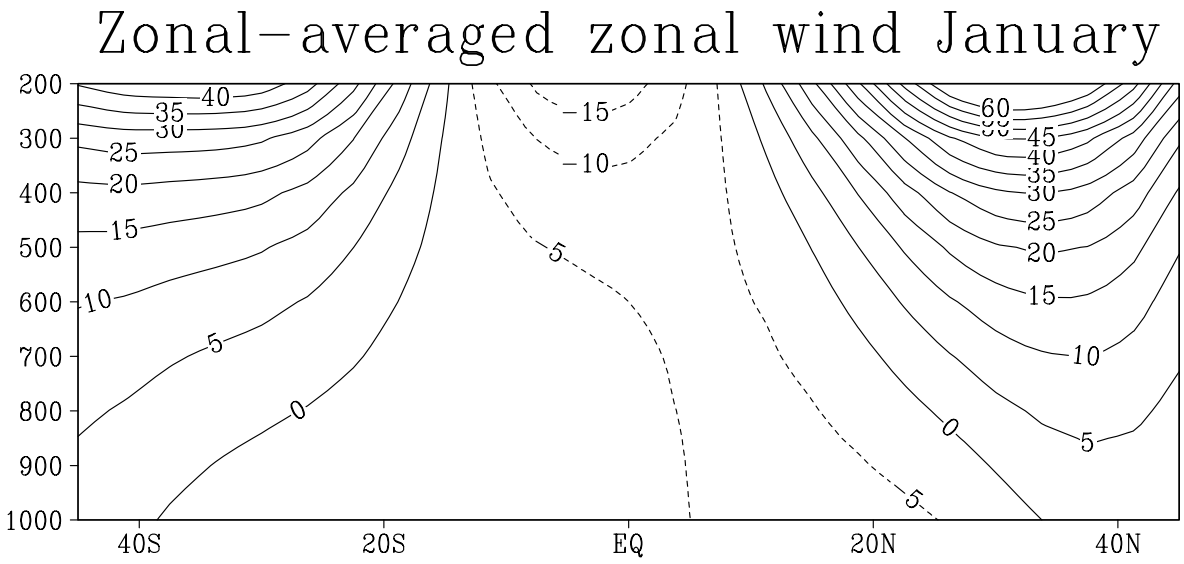

Figure 5: Model simulated January zonal averaged zonal wind. In m s^{-1}.

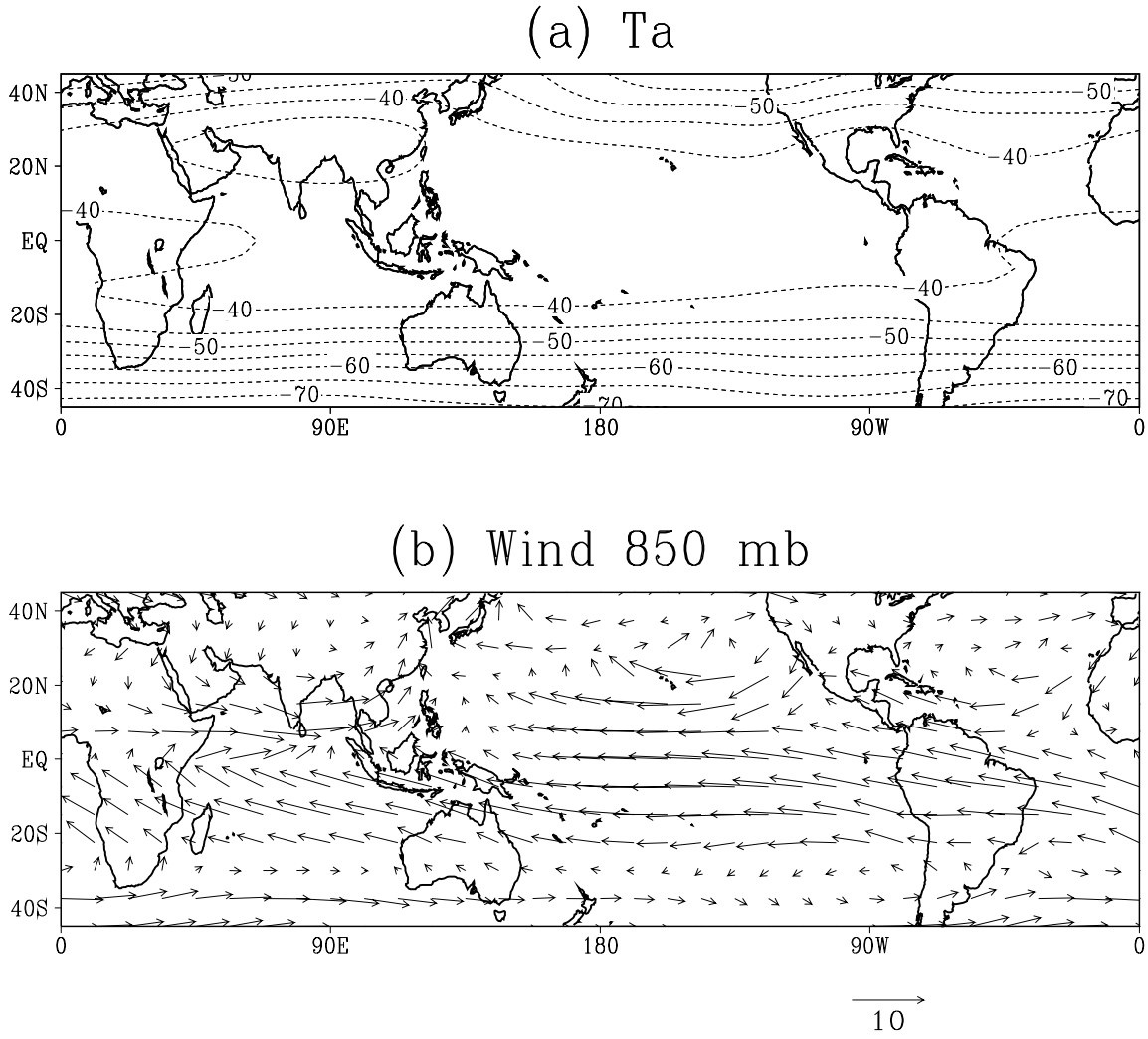

Figure 6: Model July climatology: (a) air temperature averaged between 500mb and 200mb, contour interval 5°C ; (b) 850mb winds, in m s^{-1}.

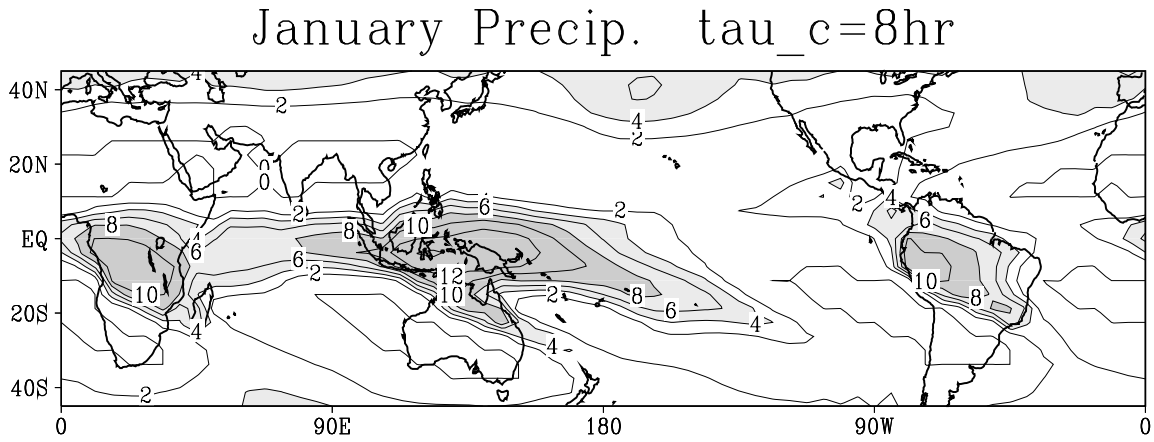

Figure 7: January climatological precipitation as in Fig. 2a, but from a run with the convective adjustment time τ_c=8 hours (2hrs in control).

Figure 8: Time-longitude plot of equatorial (averaged from 7.5°S to 7.5°N) daily mean anomalies of 850 hPa zonal wind (contour 0.5 m s^{-1}) for the control run. Negative anomalies are dotted. From January to December.

Figure 9: Power spectral density (PSD) of equatorial (average 7.5°S–7.5°N) daily mean anomalies of 850 hPa zonal wind for (a) the control run, (b) evaporation-wind feedback (EWF) suppressed, (c) extratropical excitation suppressed, and (d) both EWF and extratropical excitation suppressed. Units of $(\mathrm{m\ s^{-1}})^2$ day. Standard deviation of PSDs is 10%.

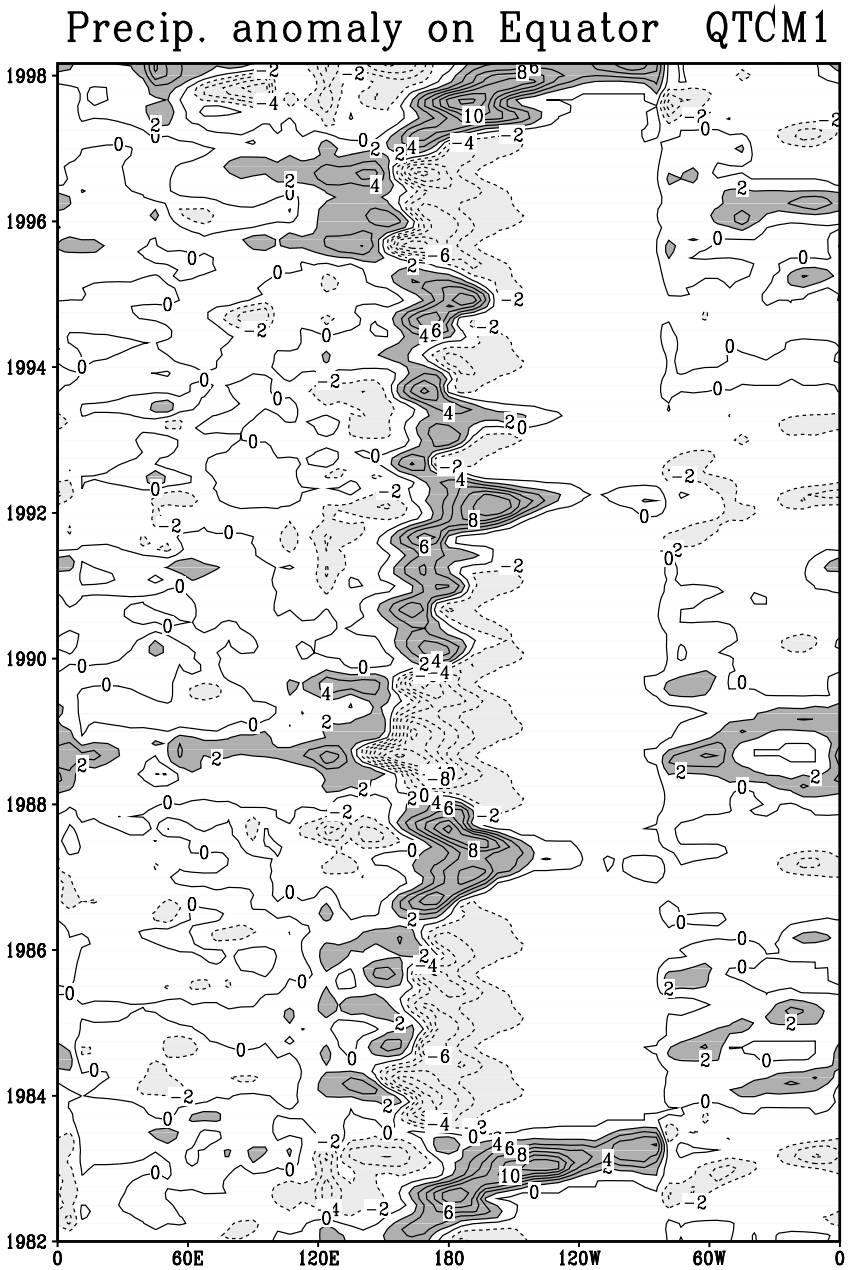

Figure 10: Model simulated monthly mean precipitation on the equator through the period 1982-1998. Contour interval 2 mm day^{-1}, with dark shading above 2 and light shading below -2.

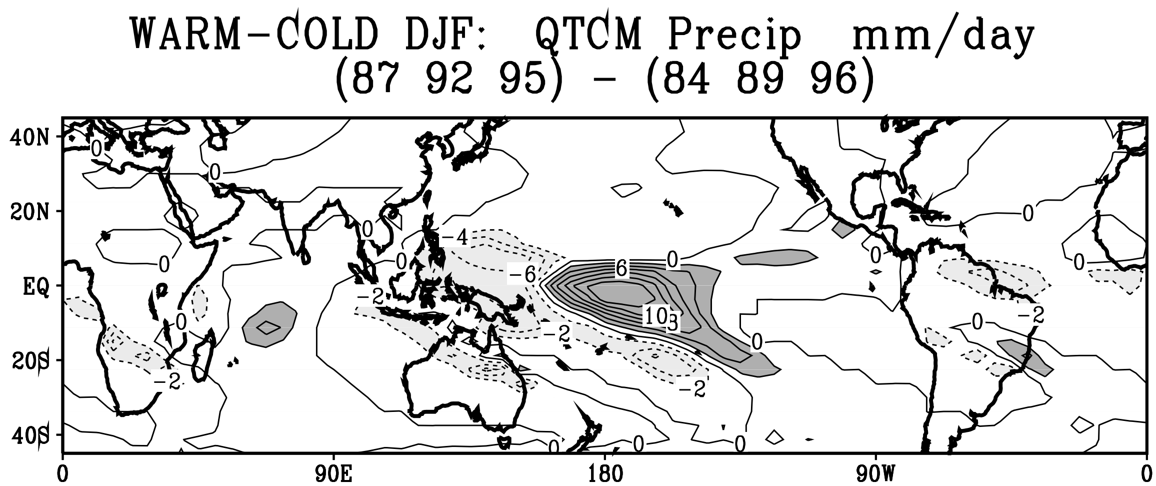

Figure 11: Winter (Dec.-Feb.) ENSO composite precipitation difference. Three warm events (86-87, 91-92, 94-95) minus three cold events (83-84, 88-89, 95-96). Contour interval 2 mm day^{-1}. Dark shading above 2 and light shading below -2 mm day^{-1}.

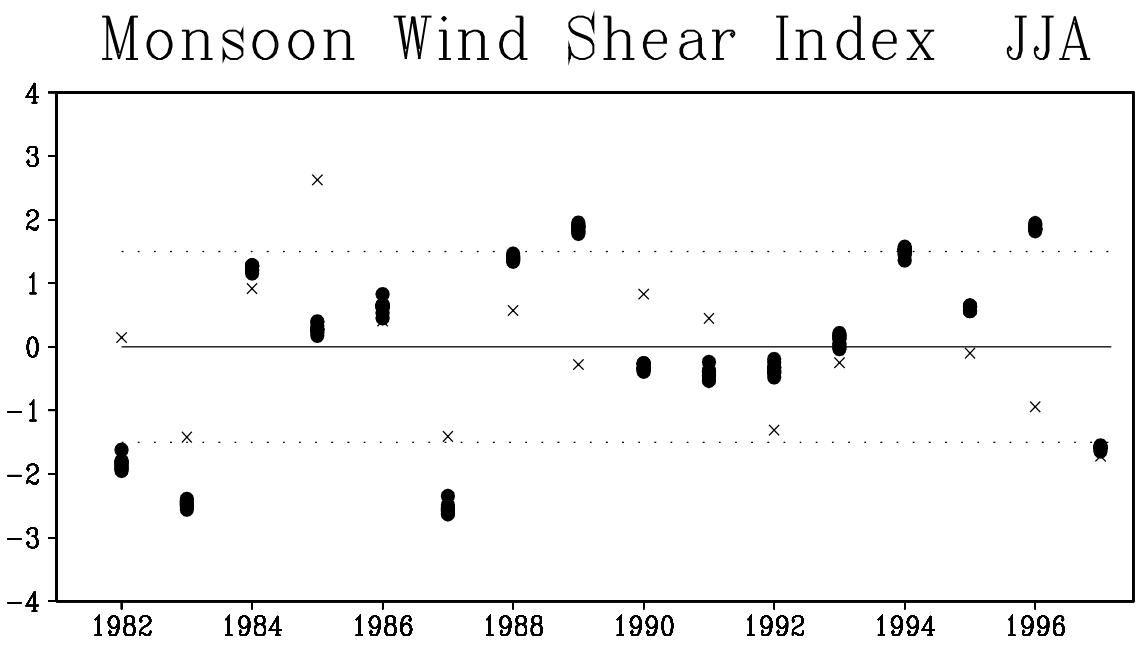

Figure 12: Interannual variation of the Monsoon Wind Shear Index (difference between the winds at 850mb and 250mb over the region 0N-20N/70E-120E) as defined by Webster and Yang (1992) for the months June-August. Filled circles are results from an ensemble of 10 model runs differing only by their initial conditions, while crosses are results from NCEP/NCAR reanalysis.

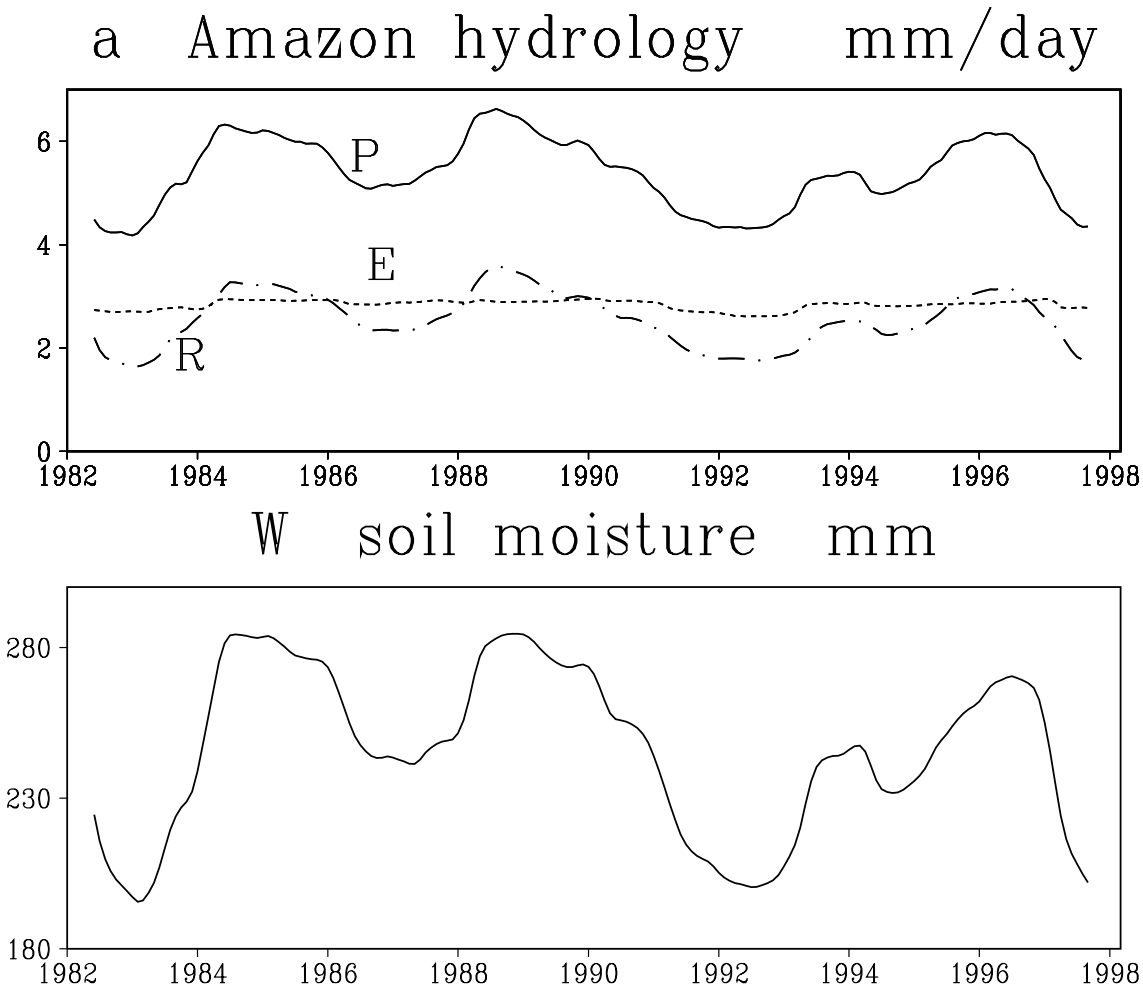

Figure 13: Interannual variations of the hydrologic cycle over the Amazon basin: (a) precipitation P (solid line), evaporation E (dashed line), runoff R (dash-dotted line), all in mm day^{-1}; (b) soil moisture content W, in mm. The monthly data are low-pass filtered by a 12 month running mean.